DEM-Assisted RFM Block Adjustment of Pushbroom Nadir Viewing HRS Imagery

Yongjun Zhang, Yi Wan, Xinhui Huang, and Xiao Ling

***Abstract*—Nadir viewing satellite image is an effective data source to generate orthomosaics. Because of the georeferencing error of satellite images, block adjustment is the first step of orthomosaic generation over a large area. However, the geometric relationship of the neighboring orbits of the nadir viewing images is not rigid enough. This paper proposes a new rational function model (RFM) block adjustment approach that constrains the tie point elevation to enhance the relative geometric rigidity. By interpolating the elevations of tie points in a digital elevation model (DEM) and estimating the *a priori* errors of the interpolated elevations, better overall relative accuracy is obtained, and the local optimal solution problem is avoided. By constraining the adjusted model parameters according to the *a priori* error of RFMs, block adjustment without ground control point (GCP) is performed. By optimal initializing the object–space positions of tie points with multi-backprojection method, the needed iteration times of block adjustment are reduced. The proposed approach is investigated with 46 Ziyuan-3 sensor-corrected images, a 1:50 000 scale DEM, and 586 GCPs. Compared with Teo's approach that constrains the horizontal coordinates and elevations of tie points, the approach in this paper converges much faster when the GCPs are sparse, and meanwhile, the absolute and relative accuracy of the two approaches are almost the same. The result of block adjustment with only four GCPs shows that no accuracy degeneration occurred in the test area and the root-mean-square error of independent check point reaches about 1.5 ground resolutions. Different DEMs and number of tie points are used to investigate whether the block adjustment result is influenced by these factors. The results show that better DEM accuracy and denser tie points do improve the accuracy when the images have large side-sway angles. The proposed approach is also tested with 5118 IKONOS-2 images that cover the southern Europe without GCP. The result shows that the relative mosaicking accuracy is much better than that of Grodecki's approach.**

***Index Terms*—Block adjustment, digital elevation model (DEM), pushbroom satellite image, rational function model (RFM).**

I. Introduction

DIGITAL orthophoto maps (DOMs) are widely used in industries such as environmental protection, energy, mining, agriculture, and civil engineering. As the spatial resolution and direct georeferencing accuracy of satellite images become higher and higher, more and more users take them as the data source for DOM producing to save cost. Nowadays, the georeferencing accuracy provided by the satellite altitude and positioning system can reach the 10-m level or even the meter level. However, it is still several times larger than the ground sample distance (GSD) of most of the high-resolution satellite (HRS) images. Thus, the geometric correction is still necessary for orthomosaic generation and mapping applications over a large area.

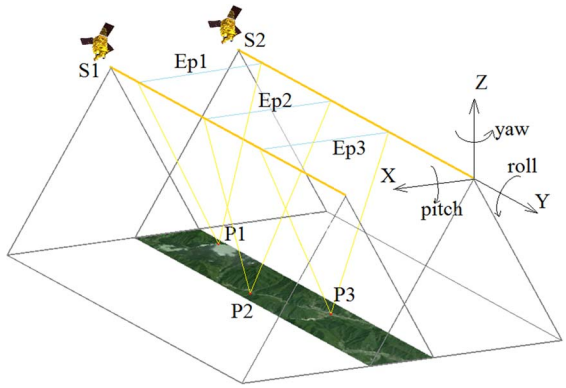

Fig. 1. Ideal geometric relationship of two neighboring nadir orbits, S1 and S2, in which the epipolar planes Ep1, Ep2, and Ep3 of tie points P1, P2, and P3 are parallel. Thus, even if the orbit S2 significantly moves in the direction of X or Z, or rotates around the axis Y in relation to S1, the rays of the tie points will converge with small residual errors. This means that the convergence of tie points cannot constrain the relative position and altitude of the orbits S1 and S2.

Block adjustment is an effective method of the geometric correction that can use sparsely distributed ground control points (GCPs) to refine HRS images over a large area. Block adjustment can also improve the relative accuracy of HRS images so that homogeneous and accurate orthomosaic over large areas can be obtained. The block adjustment procedure has already been applied to satellite images with physical camera models [1]–[4] or empirical models [5]–[9].

However, when the block adjustment data sets are only the nadir viewing (single-line-array) images, the problem is more complicated, because the geometric relationship of the neighboring single-line-array orbits is less stable than that of in-track stereo image pair. Fig. 1 illustrates the ideal geometric relationship of two single-line-array orbits, which is close to most of the real situation, i.e., the neighboring orbits have parallel scanning planes. In this situation, however, the altitudes of the camera rotate in the parallel scanning plane, and the corresponding points of the two orbits remain convergent in some place. In other words, the relative altitude and location

Manuscript received April 27, 2015; revised July 9, 2015; accepted August 4, 2015. Date of publication September 11, 2015; date of current version January 19, 2016. This work was supported in part by the National Natural Science Foundation of China under Grant 41322010 and Grant 41571434 and in part by the National High-Tech Research and Development Program under Grant 2013AA12A401.

Y. Zhang, Y. Wan, and X. Ling are with the School of Remote Sensing and Information Engineering, Wuhan University, Wuhan 430079, China (e-mail: zhangyj@whu.edu.cn; yi.wan@whu.edu.cn; zyl_whu@163.com).

X. Huang was with the School of Remote Sensing and Information Engineering, Wuhan University, Wuhan 430079, China. He is now with StarGIS Co., Ltd., Tianjin 300384, China (e-mail: huangxh@whu.edu.cn).

Color versions of one or more of the figures in this paper are available online at http://ieeexplore.ieee.org.

Digital Object Identifier 10.1109/TGRS.2015.2472498

of such neighboring orbits cannot be constrained by the convergence condition of the corresponding points. In the block adjustment, this kind of geometric instability will cause ill-conditioned normal equations if GCPs are not distributed in both orbits. While for orbits of in-track stereo image pairs, this situation will never happen because their scanning planes have relatively large angles for stereo observation.

In the previous research studies, the single-line-array orbit orientation problem was considered to be caused by weak convergence geometry, in which the base–height ratios are so small that even a little horizontal bias can lead to a large elevation bias. To solve this problem, Toutin [10]–[13] proposed a method using elevation constrained tie points (ETPs) in the block adjustment and tested the method with Landsat-7 Enhanced Thematic Mapper Plus images, pushbroom HRS stereo images, and synthetic aperture radar images. His investigations showed that good results can be obtained even if some of the involved images do not have GCP. Teo *et al.* [9] proposed a method that constrains the ground position of tie points in the block adjustment. The ground positions are obtained by ray tracing with a digital elevation model (DEM). His investigations showed that block adjustment with reduced number of GCPs can reach good absolute accuracy and good relative mosaicking accuracy. Wang *et al.* [14] tested the method of planar block adjustment with DEMs on the Chinese Ziyuan-3 (ZY-3) panchromatic nadir images and reached similar horizontal accuracy with three-line-array stereo block adjustment.

In the block adjustment problem with sensor-corrected nadir images, all the three aforementioned methods can improve the inner geometric rigidity, because the block adjustment forces the rays of tie points to be intersected on the surface of the DEM that is also used for orthorectification. However, there still remain some questions, to our knowledge, to be deeply studied before these methods can be used in real applications.

1) How to perform block adjustment of the single-line-array images without GCP?
2) How to estimate the weights of elevation constraints during block adjustment iterations? It is important because too large weights may lead the block adjustment to fall in local optimal, and too small weights cannot make the geometry rigid enough.
3) The robustness of the geometric relationship between the neighboring single-line-array orbits needs to be studied in two aspects. One is evaluating the accuracy degeneration when the GCPs are reduced. The other is evaluating the orthomosaic accuracy of the result of the block adjustment without GCP.
4) Will the elevation accuracy of block adjustment be influenced when using inaccurate DEMs? In most situations, the DEM is not as accurate as the elevation of the GCPs.

This paper will thus give the analysis and solution to the aforementioned questions. In Section II, the mathematical model of the proposed block adjustment with or without GCPs is described. The proposed approach is applied with rational function models (RFMs). In Section III, the workflow of the proposed approach is given; the initialization of tie points and the criterion of accuracy evaluation are described in detail. The proposed approach is tested with Chinese ZY-3 satellite images [3], [15], 1:50 000 scale standard DEM, and 586 high-accuracy GCPs in Section IV. In Section V, the proposed approach is also validated by block adjusting 5118 IKONOS-2 [16] images without GCP. Finally, the conclusion and some suggestions for production are given.

II. Mathematical Model of RFM Block Adjustment

A. RFM Block Adjustment Model

RFM has been universally accepted and validated as an alternative sensor orientation model for HRS imagery by now. An RFM is the ratio of two cubic polynomials with 80 rational polynomial coefficients (RPCs), which can describe the geometric relationship between a normalized object point and its corresponding image coordinates [17].

RFM is independent of sensors, mathematically simple, and computationally fast. The RPCs provided by satellite imagery manufacturers are usually derived without ground control information. Thus, the inherent biases of satellite orbit and attitude are introduced into the RPCs. However, photogrammetric block adjustment with the RPCs has been considered unfeasible because of the overparameterization [6], [7].

Thus, the proposed RFM block adjustment approach uses the adjustment model described in [6], i.e., RFM is used to express the initial relationship between object–space and image–space; the RPCs remain unchanged in the block adjustment; the adjusted function is the image–space affine transformation model. The paper of Grodecki has demonstrated that the image–space affine model is directly related to the geometric properties of the physical camera model and is numerically more stable than the traditional adjustment of exterior and interior orientation parameters.

B. Observation Equations

The proposed RFM block adjustment is a nonlinear least squares problem. The details of the way of constructing, linearizing, and solving this problem can be referred in [6]. In this section, for ease of introducing the difference of the proposed approach, the problem is described as an optimization problem that aimed to find the affine parameters and ground point positions that minimize the weighted sum of squares of the residual errors. The problem is denoted by

$$\min_{\mathbf{x}} \frac{1}{2}\boldsymbol{\varepsilon}^T \mathbf{P}\boldsymbol{\varepsilon} \tag{1}$$

where $\boldsymbol{\varepsilon} = [\varepsilon_{ij}\ \varepsilon_i\ \varepsilon_j]^T$ is the residuals; the subscripts i and j are the indices of ground point and image; ε_{ij} is the residual of the image point observation of the ith point on the jth image; ε_i is the residual of the ith ground observation; and ε_j is the residual of the pseudo-observation of the jth image model. The weight matrix $\mathbf{P}$ is a diagonal matrix. The weights p of the observation equations are calculated by

$$p = \sigma_0^2/\sigma^2 \tag{2}$$

where σ are the *a priori* errors of the observations, and σ_0 is the error of unit weight.

The solution $\mathbf{x} = [\mathbf{T}_j^T\ \cdots\ \mathbf{X}_i^T\ \cdots]^T$ of the problem includes $\mathbf{T}_j = [a_s^j\ a_l^j\ a_0^j\ b_s^j\ b_l^j\ b_0^j]^T$ (image–space affine model

parameters) and $\mathbf{X}_i = [\phi_i \ \lambda_i \ h_i]^T$ (the adjusted object–space coordinates in longitude, latitude, and height).

The observation equation of the image point is denoted by

$$\varepsilon_{ij} \begin{bmatrix} \hat{\mathbf{x}}_{ij}^{nT} & \mathbf{O} \\ \mathbf{O} & \hat{\mathbf{x}}_{ij}^{nT} \end{bmatrix} \cdot \mathbf{T}_j - \left(\mathbf{x}_{ij} - \mathbf{x}_{ij}^n\right), \text{ weight} : \mathbf{P}_{ij} \quad (3)$$

where $\mathbf{x}_{ij}^n = [s_{ij}(\mathbf{X}_i) \ l_{ij}(\mathbf{X}_i)]^T$ is the nominal image location, and $\hat{\mathbf{x}}_{ij}^n = [\mathbf{x}_{ij}^{n\,T} \ 1]^T$ is its homogeneous representation; $\mathbf{x}_{ij} = [s_{ij} \ l_{ij}]^T$ is the measured image location. The weights are estimated by (2) with the *a priori* error of the matched image observations $\sigma_{s_{ij}}, \sigma_{l_{ij}}$.

The pseudo-observation equation of the ith ground control or tie point is denoted by

$$\boldsymbol{\varepsilon}_i = \mathbf{X}_i - \mathbf{X}_i^c, \text{ weight} : \mathbf{P}_i \quad (4)$$

where $X_i^c = [\phi_i^c \ \lambda_i^c \ h_i^c]^T$ is the measured ground position; and $\boldsymbol{\varepsilon}_i = [\varepsilon_{\phi_i} \ \varepsilon_{\lambda_i} \ \varepsilon_{h_i}]^T$ is the residual error in longitude, latitude, and elevation. For GCPs, all the three pseudo-observation equations are added, and the weights are calculated by the *a priori* error $(\sigma_\phi, \sigma_\lambda, \sigma_h)$ of the measured ground position. However, for tie points, only the third equation that constrains the elevation is added. The way of estimating the *a priori* error $\sigma_{\nabla H}$ of the elevation of a tie point will be described in the next section.

If the *a priori* georeferencing error of the HRS images is already known, the pseudo-observation equations of the affine parameters can also be added as

$$\boldsymbol{\varepsilon}_j = \mathbf{T}_j - \mathbf{O}, \text{ weight} : \mathbf{P}_j \quad (5)$$

where $\boldsymbol{\varepsilon}_j$ is the residual error of the affine model parameters, and $\mathbf{O}$ is a zero vector that represents the initial affine model parameters. This idea is previously used in the GPS-aided photogrammetric bundle adjustment in which exposure positions obtained by airborne GPS are treated as weighted observations. Since RFM is an approximation of the physical camera orientation model that is obtained by the satellite-borne GPS and gyros, the initial affine model parameters can also be treated as weighted pseudo-observations, which provides weak constraints on the camera location and attitude. The constraints can avoid the georeference of images varying too much in the block adjustment without GCPs. The pseudoweight value of the affine model parameters should be set according to the *a priori* georeferencing accuracy of the initial satellite images (most commercial satellite images have public nominal geometric accuracy), i.e.,

$$\sigma = \begin{cases} \sigma_j/(G_j), & \text{for } a_0^{(j)} \text{ and } b_0^{(j)} \\ \sigma_j/(G_j \cdot W_j), & \text{for } a_s^{(j)} \text{ and } b_s^{(j)} \\ \sigma_j/(G_j \cdot H_j), & \text{for } a_l^{(j)} \text{ and } b_l^{(j)} \end{cases} \quad (6)$$

where σ_j is the *a priori* georeferencing error of the jth RFM; G_j is the GSD of the jth image; and W_j and H_j are the width and height in pixels of the jth image.

C. Estimation of the Elevation A Priori Error of Tie Points

In the work of Teo *et al.* [9], the *a priori* error of the elevations of tie point is set ten times that of GCPs. In the work of Wang *et al.* [14], the elevations of tie point are treated as truth values in the adjustment equations of each iteration. However, a large initial satellite georeferencing error may cause a large error in the initial elevations of tie point in mountainous areas, which may lead the adjustment to a local optimal. To weaken the influence of the initial error in such situations, the weight value of the elevations is set by estimating the *a priori* error of the elevations of tie point in the proposed approach.

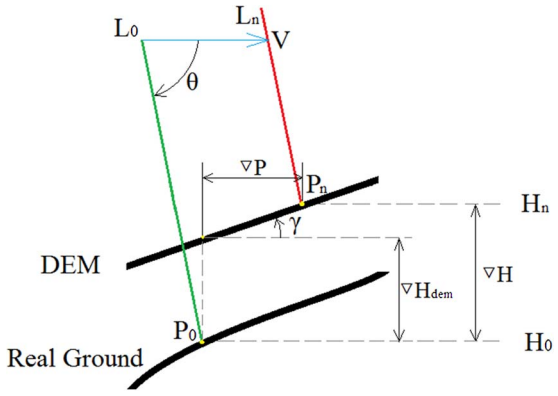

Fig. 2. Error lies in the elevations of multiray backprojection. L_0 is the accurate ray, and P_0 is its projection on the real ground. L_n is the ray in which the direct geoposition error lies, and P_n is its projection on the DEM. Thus, P_0 is the real ground position, and P_n is the ground position estimated by single- or multiray backprojection. V is the direction of the georeferencing error, and γ is the slope angle of the DEM in this direction.

The elevation error source of a certain tie point is illustrated in Fig. 2. The elevation error is mainly caused by the DEM and horizontal errors of tie point. To simplify the deduction, it is assumed that the gradient in the DEM remains unchanged within the range of the horizontal error. Thus, the elevation error is denoted by

$$\nabla H = H_0 - H_n = \nabla H_{\text{DEM}} + \nabla P \cdot \tan\gamma \quad (7)$$

where ∇H_{DEM} is the DEM error at the true position P_0 of the tie point; ∇P is the horizontal distance between the true position P_0 and the back projected position P_n; and γ is the slope angle of the DEM at the position P_0.

In the proposed approach, the elevation *a priori* error of tie point is estimated under the following assumptions.

1) The DEM error belongs to the Gaussian distribution.
2) The georeferencing error is a constant in the test area.
3) The slope $\tan\gamma$ in the direction of the georeferencing error belongs to the Gaussian distribution.

The *a priori* error of elevation of tie point is calculated by

$$\sigma_{\nabla H} = \sqrt{\sigma_{\text{DEM}}^2 + (\nabla P \cdot \sigma_{\tan\gamma})^2} \quad (8)$$

where σ_{DEM} is the *a priori* RMSE of the DEM, and $\sigma_{\tan\gamma}$ is the RMS of the slope $\tan\gamma$.

The *a priori* RMSE of national standard DEM products is usually easy to be inquired. If no standard DEM is available, the Shuttle Radar Topography Mission (SRTM) DEM can be used. The accuracy of the SRTM has also been extensively studied [18], [19]. The RMSE of the slope $\tan\gamma$ of the DEM is computed before the block adjustment.

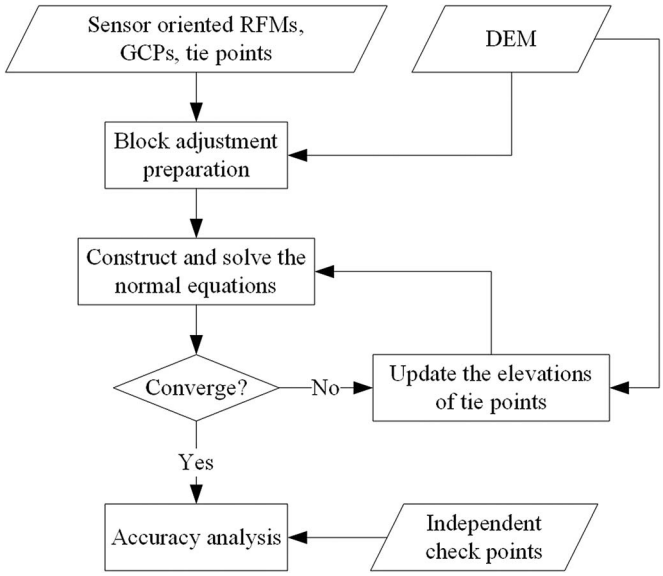

Fig. 3. Workflow of the proposed block adjustment approach.

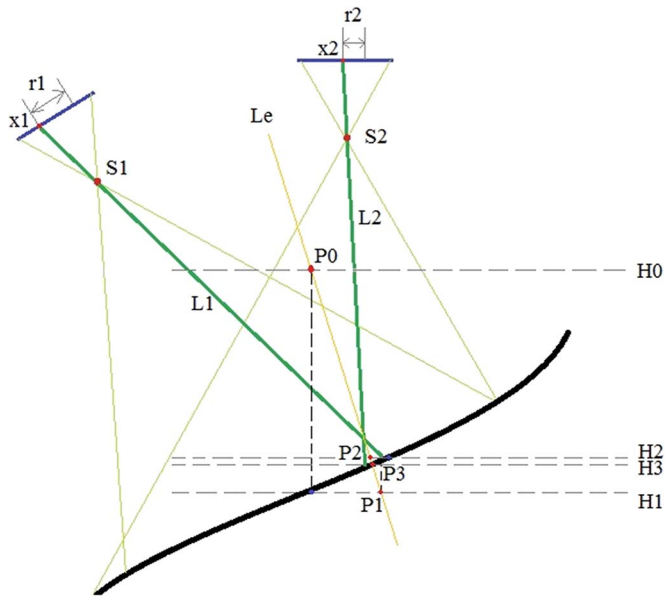

Fig. 4. Multiray backprojection. S1 and S2 are the perspective centers, x1 and x2 are the image points, r1 and r2 are the RMS, and L1 and L2 are the rays of the image coordinates of x1 and x2. Le is the equivalent ray of L1 and L2. H_i and P_i are the given elevations and the computed position of the tie point during the iterative backprojection.

D. Solution of the Block Adjustment Problem

In the proposed approach, the Levenberg–Marquardt (LM) algorithm [20] is used for solving this nonlinear least squares problem. The Schur compliment trick [21] is used to reduce the normal equations for saving the internal memory of the computer, because the unknown vector has a block structure and the blocks are not correlated. The Cholesky factorization method is used to solve the small-scale problems with less than 1000 images. For large-scale problems with more than 1000 images, the normal equations are solved by an iterative linear solver called the conjugate gradients method [22]. Since there are a lot of literatures introducing these optimization solvers, the theoretical foundations and detailed algorithms will not be described in this paper.

III. Workflow of the Proposed Approach

A. Workflow of the Proposed Approach

The workflow of the proposed approach is illustrated in Fig. 3, which includes three parts.

1) Block Adjustment Preparation: The goal is to prepare the data for block adjustment. The image points of ground control or tie points should be checked for eliminating obvious errors. The ground coordinates of the tie points should be initialized according to Section III-B.

2) Adjustment Iterations: First, the linear least squares problem of the LM algorithm is constructed and solved. Then the unknowns are updated with the adjusted solution. Second, the convergence of the block adjustment is checked. The convergence depends on both the change of the cost function [in (1)] and the change of RMSE of GCPs. Only if both the changes are smaller than their given thresholds, the block adjustment iteration will be terminated. The iteration is also terminated if the maximum iteration number is reached. If the termination condition is not reached, then the process goes to the third step. Third, the elevations of tie points are interpolated at the updated horizontal positions. If GCPs are available, the *a priori* errors of the elevations of tie points should also be calculated as described in Section II-C.

TABLE I
Options and Settings of the Proposed Approach

Items		Values
a priori error	unit weight	$\sigma_0 = 1m$
	image observes of tie points	$\sigma_p = \sigma_l = 1\ pixel$
	image observes of GCPs	$\sigma_p = \sigma_l = 0.5\ pixel$
	horizontal position of GCPs	$\sigma_\phi = \sigma_\lambda = 2m$, $\sigma_h = 3m$
	sensor-oriented RFMs	$\sigma_i = 100m$
	1:50,000 DEM	$\sigma_{DEM} = 10m$
	SRTM	$\sigma_{DEM} = 50m$
threshold for termination	change of $\varepsilon^T P\varepsilon$	10^{-5}
	change of GCP RMSE	$10^{-5}m$
	maximum iteration number	100

3) Accuracy Evaluation: The absolute and mosaicking errors are evaluated with independent check points (ICPs) and tie points. The way of evaluation is described in Section III-C.

B. Tie Point Position Initialization

Since weak convergence geometry usually exists in the block adjustment of single-line-array HRS images, the ground positions of tie points may be inaccurate if they are calculated by space intersection. The initialization of tie points should be aided by DEM. In Teo's work, each of the image correspondences of a tie point is used for obtaining a ground position by the ray-tracing algorithm. Then, the initial position of the tie point is

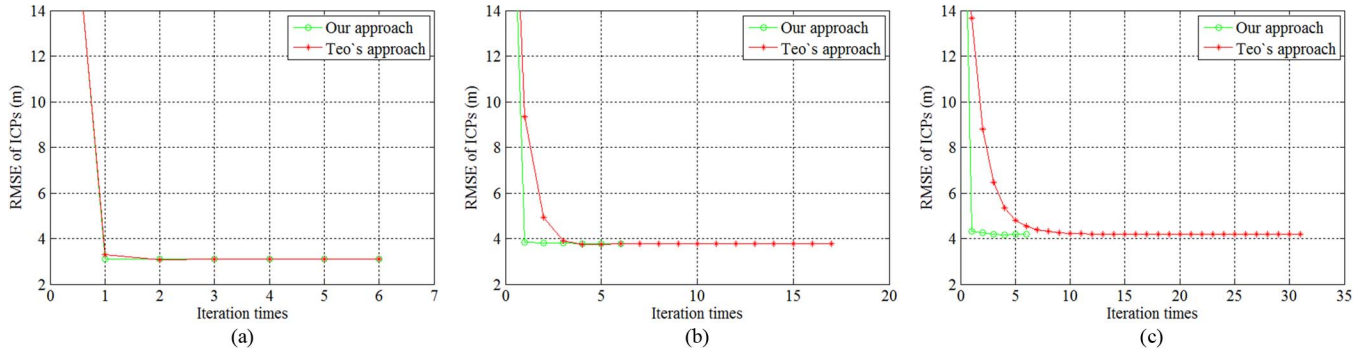

Fig. 5. Horizontal RMSE of ICPs in the iteration of block adjustments. Different numbers of GCPs are involved. As the number of GCPs decreases, Teo's approach needs more and more iterations to converge. However, the iteration times of our approach are almost not influenced by the number of GCPs. In Teo's approach, the ICPs are moved gradually from the initial positions to the final positions. However, in our approach, the ICPs can reach the final position at the first iteration. (a) Sixty-four GCPs are involved. (b) Twelve GCPs are involved. (c) Four GCPs are involved.

calculated by averaging the ground positions of its image correspondences. This method works in most situations [23], [24].

The elevation is calculated by multiray backprojection in the proposed approach. The procedure of this method is illustrated in Fig. 4. This method solves the following optimization problem in each of the backprojection iterations (the elevation is known):

$$\min_{[\phi_i\ \lambda_i]^T} \frac{1}{2}\varepsilon_i'^T \mathbf{P}_i' \varepsilon_i' \tag{9}$$

where ε_i' is the residual vector of the ith tie point, $\mathbf{P}_i'$ is the weight matrix, and $[\phi_i\ \lambda_i]^T$ is the unknown vector. The residual vector of the jth image correspondence of the ith tie point is denoted by

$$\varepsilon_{ij}' = \mathbf{x}_{ij}^n - \mathbf{x}_{ij},\ \text{weight}\ \mathbf{P}_{ij}'. \tag{10}$$

The weights of the image observations do not depend on the *a priori* error of image matching. They depend on the *a priori* georeferencing error of the RFM. The advantage of this method is that the initial positions of tie points are optimal even when the involved images have different georeferencing accuracy values. The LM algorithm and Cholesky factorization are used to solve the optimization problem.

C. Accuracy Analysis

When GCPs are available, the absolute accuracy of block adjustment result can be evaluated by the RMSE of the ground coordinate disparities. However, the possible weak convergence geometry will cause that the ground position cannot be calculated accurately by space intersection. Thus, in the proposed approach, only absolute horizontal accuracy is evaluated. The nominal horizontal location of a GCP is calculated by multiray backprojection (see Section III-B) with its known elevation.

In the proposed approach, GCPs that have more than one image correspondence are also used to evaluate the mosaicking error. The way of calculating the mosaicking error is denoted by

$$m_{x_i} = \sqrt{\frac{1}{n}\sum_{j=1}^{n}(\nabla x_{ij} \cdot G_j)^2} \quad m_{y_i} = \sqrt{\frac{1}{n}\sum_{j=1}^{n}(\nabla y_{ij} \cdot G_j)^2} \tag{11}$$

TABLE II
ABSOLUTE ACCURACY

Items		Our approach	Teo's approach
64 GCPs	horizontal RMSE of GCPs (m)	3.007	3.007
	horizontal RMSE of ICPs (m)	3.096	3.096
	iteration times	6	6
12 GCPs	horizontal RMSE of GCPs (m)	3.165	3.165
	horizontal RMSE of ICPs (m)	3.791	3.790
	iteration times	6	17
4 GCPs	horizontal RMSE of GCPs (m)	3.512	3.507
	horizontal RMSE of ICPs (m)	4.179	4.187
	iteration times	6	31

where m_{x_i} and m_{y_i} are the mosaicking errors in sample (cross-track) and line (in-track) directions of the ith GCP; n is the number of image correspondences; ∇x_{ij} and ∇y_{ij} are the residual errors of the ith image point; and G_j is the GSD of the jth image. For a test area, the mean value of the mosaicking error of GCPs is used to evaluate the overall mosaicking accuracy.

When processing block adjustment without GCP, tie points are used to evaluate the mosaicking error in each of the image pairs. In an image pair, each of the corresponding points has two image points, and thus, two ground positions can be calculated by ray tracing with the DEM and the block adjustment result. The horizontal disparity between the two ground positions is the local mosaicking error of the corresponding point. The root of the squared mean of the horizontal disparities is used to evaluate the mosaicking accuracy of an image pair.

However, the mean horizontal disparities of tie points are strongly influenced by the DEM error. Assume no error exists in the block adjustment result, the relationship between the horizontal disparity of a tie point and the DEM elevation error is denoted by

$$m_i = 2\ \tan\frac{\phi_{j_1 j_2}}{2} \cdot \nabla H_{\mathrm{DEM}_i} \tag{12}$$

where m_i is the horizontal disparity of the ith tie point in the image pair of the j_1th image and the j_2th image; $\phi_{j_1 j_2}$ is the intersection angle of the image pair; and $\nabla H_{\mathrm{DEM}_i}$ is the

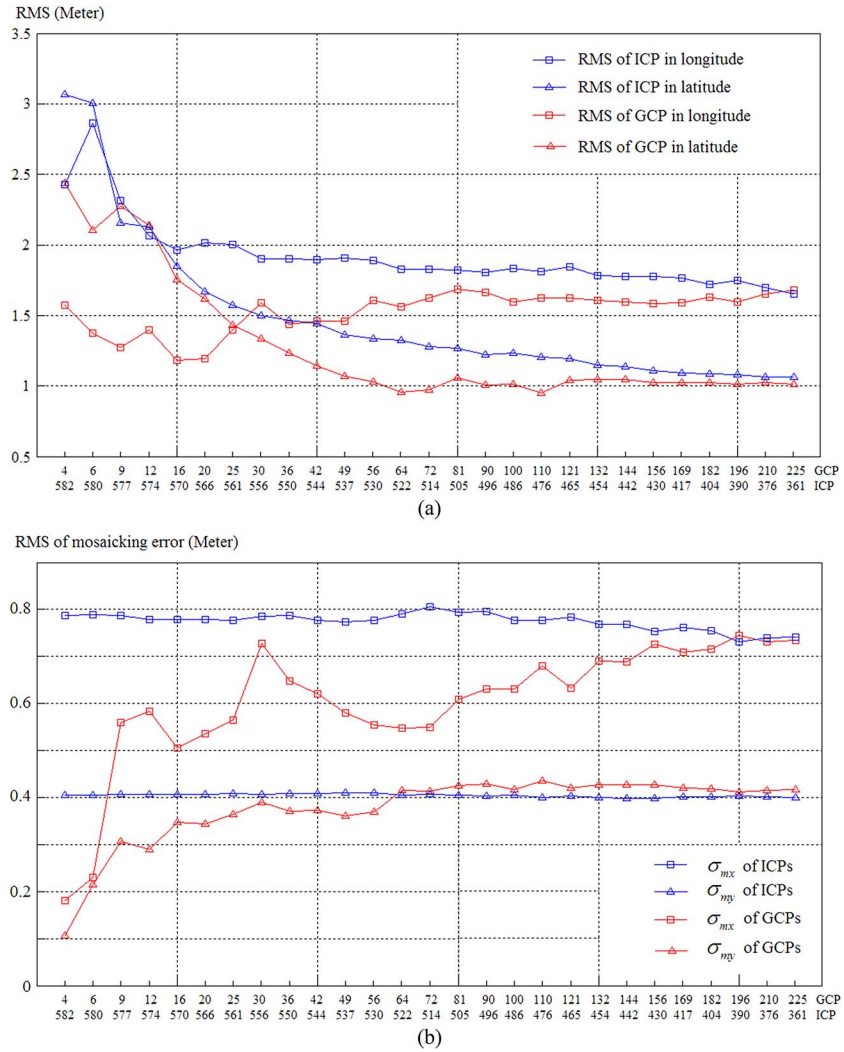

Fig. 6. Absolute and relative accuracy of block adjustment with varying number of GCPs. (a) RMS of GCPs and ICPs in the result of block adjustment with different numbers of GCPs. (b) Mean mosaicking error of GCPs and ICPs in the result of block adjustment with different numbers of GCPs.

elevation error of the DEM at the position of the ith tie point. This equation reveals that larger intersection angles and worse DEM accuracy lead to a larger mosaicking error.

IV. Validate the Proposed Approach With GCPs

There are two goals of the investigation in this section.

1) Section IV-A validates the proposed approach with GCPs in terms of the absolute accuracy, mosaicking accuracy, and robustness. Teo's approach is used for comparison.
2) Section IV-B evaluates the influences of the DEM accuracy and tie point density on the block adjustment results.

These investigations use the nadir viewing ZY-3 images from the China Centre for Resource Satellite Data and Application (CRESDA). The involved images are sensor-corrected products, on which only the radiometric correction and on-orbit calibration were performed. The GSD of the panchromatic nadir viewing ZY-3 image is about 2.1 m. The detailed properties of ZY-3 images can be referred in [3].

The involved images were acquired over Shanxi Province, China, between April 30, 2013 and August 31, 2013. There is no snow-covered area, and the cloud covering rate is less than 10% in each image. The topography in Shanxi Province is mainly mountains and covers different environments: residential, semi-rural, forested areas, and many coal mines. The elevation ranges from 500 to 3000 m. The GCPs were manually acquired from a 1:10 000 scale DOM with 2-m GSD and a 1:50 000 scale standard DEM with 25-m grid intervals. The *a priori* error of the 1:10 000 scale DOM is approximately 3 m horizontally, and the *a priori* error of the 1:50 000 scale DEM is about 3 m in the plain area and 5 m in the mountains. The SRTM DEM with 90-m grid intervals is used for comparison in Section IV-B. The *a priori* elevation error is about 20 m in the plain area and 50 m in the mountains.

TABLE III
Results of Block Adjustment With All GCPs and Without GCP

Unit: meter		Absolute accuracy		Mean mosaicking error	
		Long	Lat	Long	Lat
All GCPs	Max	6.13	4.12	3.02	1.23
	RMS	1.60	0.94	0.71	0.40
All ICPs	Max	12.88	20.90	4.35	1.25
	RMS	11.50	15.49	0.81	0.40

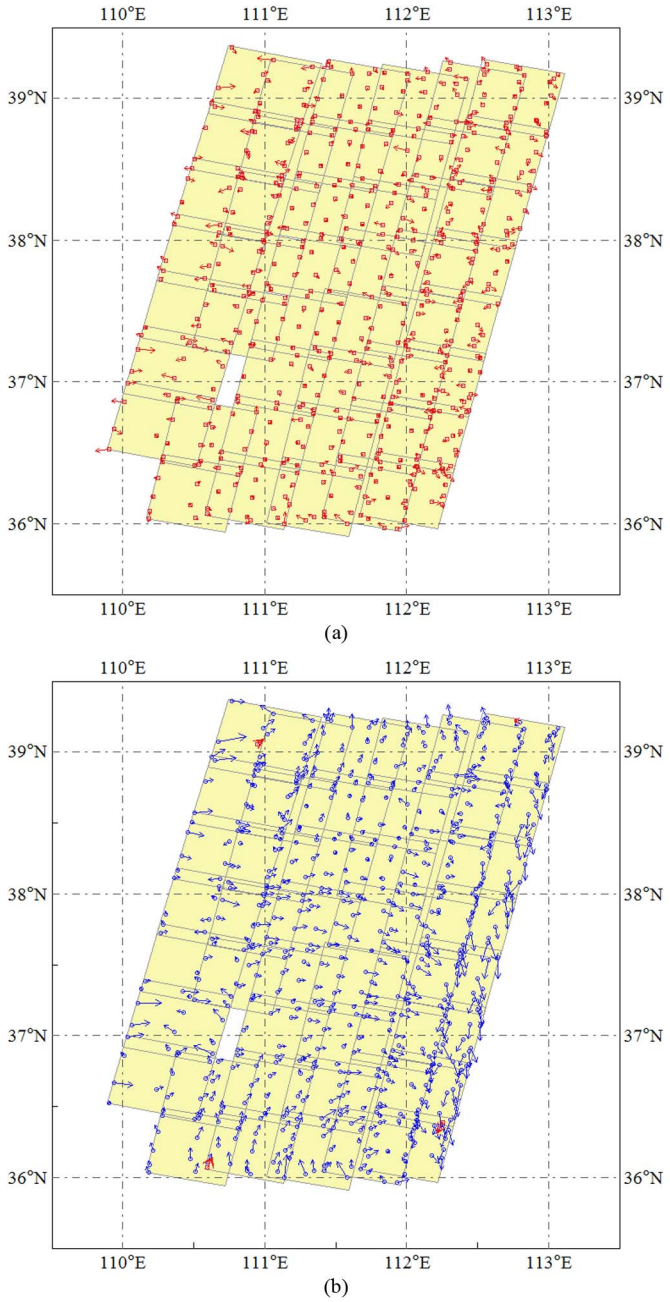

Fig. 7. Horizontal error vectors of GCPs (red squares and arrows) and ICPs (blue circles and arrows) in the results of the proposed approach. The test shown in (a) used all GCPs as control. The test shown in (b) used four GCPs as control. (a) All GCPs are used for controlling. (b) Four GCPs are used for controlling, and the others are used as ICPs.

Some important settings and options of the proposed approach in this investigation are listed in Table I. The block adjustment experiments in this section were processed in a laptop having an Intel Core-i5 CPU and 8 GB internal memory.

A. *Validation of the Proposed Approach*

In the data preparation stage for the investigation, about 2000 tie points are automatically matched in each image, and 586 GCPs are manually measured and validated. When testing Teo's approach, the ground positions of tie points are taken as pseudo-observations in each iteration, and the *a priori* error is set to be ten times that of GCPs ($\sigma_\phi = \sigma_\lambda = 20$ m, $\sigma_h = 30$ m).

TABLE IV
PROPERTIES OF IMAGE BLOCKS FOR TESTING WITH DIFFERENT DEMS

Items	Group 1		Group 2	
	Master (right)	Slave (left)	Master (right)	Slave (left)
Location	E111.8 N36.6	E111.5 N36.6	E111.1 N38.6	E110.8 N38.6
Side-sway angle (roll)	1°	1°	1°	22°
GCP number	29	-	28	-
ICP number	-	28	-	25
Overlapping rate	About 50%		About 50%	
Viewing angle	About 4°		About 23°	

Master denotes the images having GCPs. Slave denotes the image having no GCPs.

The 1:50 000 scale DEM is used for interpolating the elevations of tie points in both approaches.

Different numbers of GCPs are used for comparing the convergence speed and absolute accuracy of the two approaches. This test is performed three times with 64, 12, and 4 GCPs, respectively. Fig. 5 illustrates the horizontal RMSE of ICPs in the block adjustment iterations. The absolute accuracy is compared in Table II. The results show that the horizontal RMSEs of the GCPs and ICPs of the two approaches are almost the same. However, Teo's approach needs more iteration times to converge. As shown in Fig. 5 and Table II, the less the GCPs, the more iterations Teo's approach needs to converge. The ICPs are moved gradually from the initial positions to the final positions. However, in the proposed approach of this paper, the ICPs can reach the final position at the first iteration, no matter how many GCPs are used for control. This property makes our approach very time-efficient, particularly when outliers in the tie points are needed to be eliminated iteratively.

In order to fully evaluate the absolute and relative accuracy, the proposed approach was tested with randomly selected GCPs. The number of GCPs varied from 4 to 225. In order to avoid extrapolation, the test area was divided regularly into grids, and the GCPs are selected in each grid. The unselected GCPs were used as ICPs. In addition, the approach was also tested with all the GCPs and with no GCP.

Fig. 6 illustrates the absolute and relative accuracy of the results of the tests with 4–225 GCPs. As shown, when the GCP number decreases from 225 to 4, the RMSE of ICPs in the longitude direction increases from 1.6 m (less than 1 GSD) to 2.9 m (less than 1.5 GSD); the RMSE of ICPs in the latitude direction increases from 1.1 m (0.5 GSD) to 3.1 m (1.5 GSD); the mean mosaicking error of ICPs in the longitude direction slightly increases from 0.74 to 0.78 m; and the mean mosaicking error of ICPs in the latitude direction is not changed at about 0.40 m. These results prove that the proposed approach can reach high accuracy when using very sparse GCPs. Table III lists the absolute accuracy and mosaicking accuracy of the test using all the GCPs and no GCP. Combining the mosaicking error listed in Table III and the mosaicking error illustrated in Fig. 6(b), it is clear that the number of GCPs almost has no influence on the mean mosaicking error, which demonstrates the inner geometry of the proposed block adjustment is rigid.

Fig. 7 illustrates the horizontal error vectors of GCPs (red squares and arrows) and ICPs (blue circles and arrows). Fig. 7(a) illustrates the result of the test using all the GCPs,

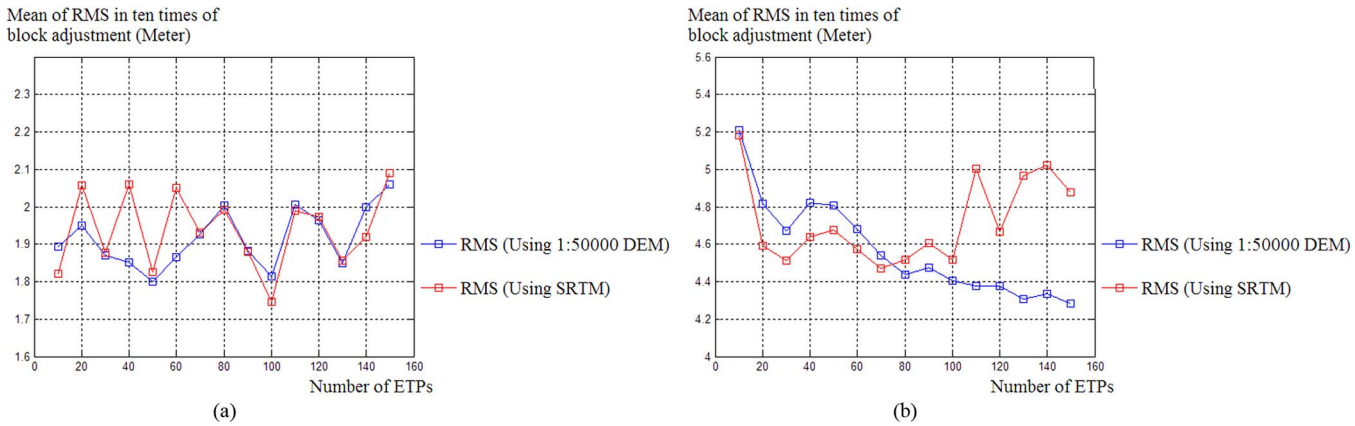

Fig. 8. Block adjustment result of the test with different DEMs and different densities of ETPs. Each node means the mean horizontal RMS in ten times of block adjustment with the corresponding number of ETPs. (a) Mean horizontal RMS of ICPs in Group 1. (b) Mean horizontal RMS of ICPs in Group 2.

and Fig. 7(b) illustrates the result of the test using the least number of GCPs (four GCPs). In Fig. 7(a), the directions of the error vectors are randomly distributed, whereas in Fig. 7(b), the directions are systematic at a certain extent. However, Fig. 7(b) also shows that the accuracy is consistent in the whole test area because the accuracy degradation does not occur in the images that are far away from the GCPs, which also demonstrates that the inner geometry of the proposed block adjustment is rigid.

B. *Influence of DEM Accuracy and Tie Point Density*

For the users who cannot obtain standard high-accuracy DEM products, the SRTM is a good choice. However, how the proposed block adjustment result is influenced by the DEM accuracy needs to be investigated. Theoretically, denser tie points can reduce the influence of the random error in their elevation constraints, but it is not supported by enough evidence. To investigate the two questions, a test was conducted with the following conditions.

1) Two groups of images were involved. Each group included two images, and the images were at different orbits. The images were selected from the mountainous region of Shanxi test area. Group 1 had a small intersection angle (4°); Group 2 had a large intersection angle (23°). The detailed information is listed in Table IV.
2) In each group, one image was used as the master image (having only GCPs), and the other was used as the slave image (having only ICPs). The RMSE of ICPs was used to evaluate the accuracy of the result.
3) The standard 1:50 000 scale DEM with 25-m grid intervals and the SRTM with 90-m grid intervals were used in this test for comparison.
4) The overlapping areas of the two groups were regularly divided into grids, and the tie points were randomly selected from them. Each selection of tie points and the following block adjustment were performed ten times to avoid the influence of random factors.

Fig. 8(a) illustrates the horizontal RMSE of ICPs in Group 1 that varies from 1.7 m to 2.1 m irregularly. So it can be concluded that the accuracy is almost not influenced by the number of tie points and the accuracy of the DEM. Fig. 8(b) illustrates the horizontal RMSE of ICPs in Group 2. When using the standard DEM, the RMSE decreases from 5.2 to 4.2 m as the number of tie points increases from 10 to 150. When using the SRTM, the RMSE slightly decreases from 5.2 to 4.5 m as the number of tie points increases from 10 to 100, but then increases to 5.0 m as the number of tie points increases to 150. Thus, in Group 2, the accuracy of the result is influenced by both the DEM accuracy and the density of tie points.

This test demonstrates the following conclusions:

1) The DEM accuracy does not influence the accuracy of the results only when the intersection angles between the block adjusting images are all very small.
2) When block adjusting images that have larger intersection angles, using denser tie points can slightly improve the accuracy of the result.

V. Validate the Approach With Tie Points Only

The proposed approach was also validated by IKONOS-2 standard geometrically corrected images. Five thousand one hundred eighteen RFMs and about 307 000 tie points were provided by ESRI (www.esri.com) and simultaneously adjusted. A lot of GCPs are needed if the purpose is to improve the absolute accuracy of these images because they are not linked as a single network. However, only tie points on the overlapping areas are needed if the purpose is to improve the relative accuracy. The block adjustment was processed in a certain server of ESRI. The delivered RFMs were believed to have about 6-m accuracy. Thus, the options and settings of the approach are the same with those in Section IV, except that the *a priori* error of the RFMs is set 6 m ($\sigma_i = 6$ m).The images covered most part of the southern Europe (see Fig. 9). Since no GCP was available, the absolute accuracy was not assessed, and the mosaicking error was evaluated by tie points. The SRTM was used for interpolating the elevations of tie points. The proposed approach was compared with the Grodecki's RFM block adjustment, in which neither the elevations nor the horizontal positions of tie points are constrained [5]. However, to avoid the divergence, the pseudo-observations of adjusted model parameters were also added in Grodecki's approach with the same *a priori* error of the RFM.

Fig. 10(a) illustrates the histogram of the mosaicking errors of all the image pairs. Obviously, there are much more image pairs that have less than 5-m mosaicking errors in our approach when compared with those in Grodecki's approach.

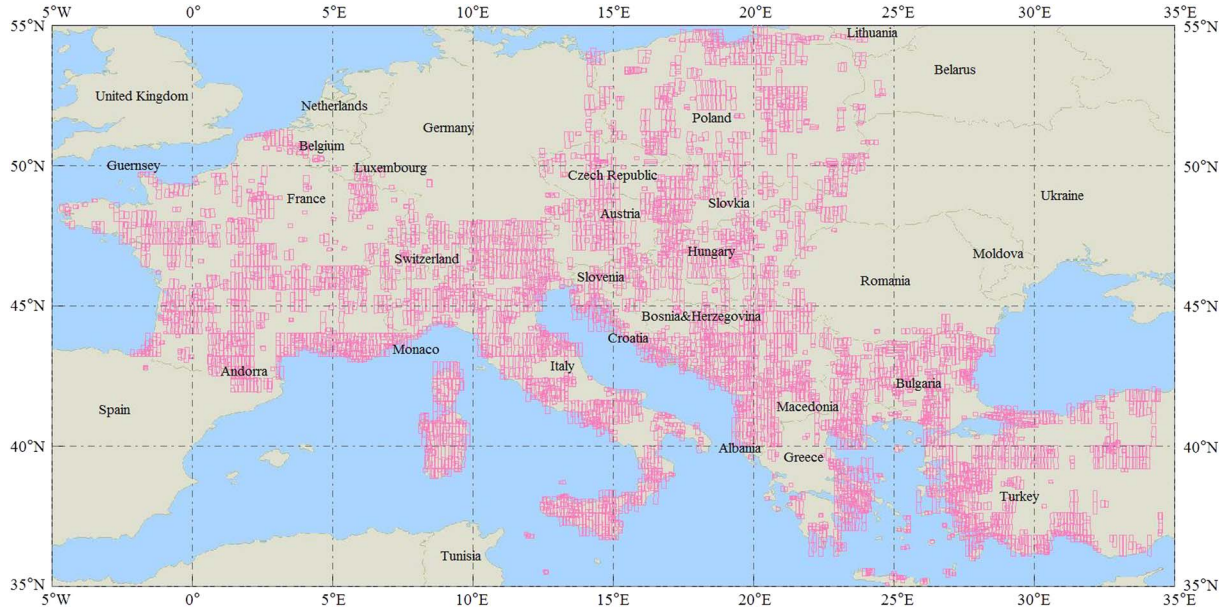

Fig. 9. European test area and outlines of the IKONOS-2 image.

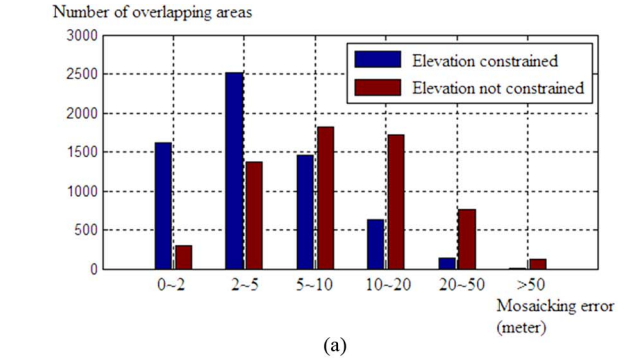

(a)

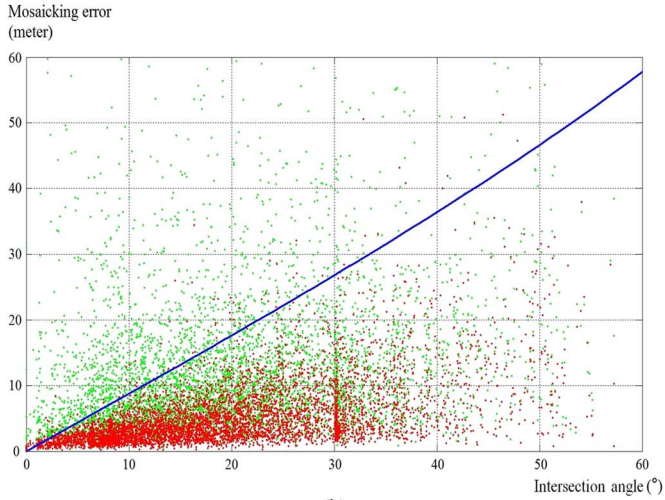

(b)

Fig. 10. Absolute and relative accuracy of block adjustment with varying number of GCPs. (a) Histogram of the mosaicking error. (b) Relationship between the intersection angle and the mosaicking error. Each point represents an image pair. Green points are the results of Grodecki's approach. Red points are the results of our approach. Blue line represents the computed mosaicking error caused by the 50-m elevation error DEM.

Fig. 10(b) illustrates the relationship between the intersection angle and the mosaicking error. Since the *a priori* error of the SRTM is believed to be less than 50 m in most areas, the mosaicking error caused only by the 50-m DEM error is treated as the maximum mosaicking error. The blue curve in Fig. 9(c) represents the maximum mosaicking error with different intersection angles [calculated by (12)]. In our approach, the mosaicking errors of almost all of the image pairs are smaller than the curve of the blue line. However, in Grodecki's approach, the mosaicking errors of many image pairs are larger than the blue curve. These experiments demonstrated that the proposed block adjustment approach is geometrically rigid when processing the IKONOS images.

VI. Conclusion

This paper analyzes the problem that existed in the orientation of neighboring nadir-viewing single-line-array satellite orbits and proposes a new RFM block adjustment approach. This paper also theoretically analyzes the error that lies in the interpolation of the elevation of tie points and proposes a weight estimation method. In the proposed approach, the pseudo-observation constraints of adjusted model parameters constrain the position of images, which plays the role of GCPs; thus, the block adjustment without GCPs is achieved, and the iteration will not diverge in such conditions. The result of experiments taking all the GCPs as ICPs in Section IV-A demonstrates that the proposed method can achieve very good relative accuracy (0.81 m in longitude and 0.40 m in latitude on the 2.1-m GSD ZY-3 nadir images) in such conditions. The robustness of the proposed approach is evaluated in the same experiment by reducing the number of GCPs (with a 3-m *a priori* horizontal error) from 225 to 4. The RMSE of ICPs changes from about 1.5 to 3 m (0.75–1.5 pixels), and the mean mosaicking error remains less than 1 m (0.5 pixels). In Section IV-B, the experiment using different DEMs demonstrates that the *a priori* error of the DEM can influence the accuracy of the result when the convergence angles are very large. In Section V, the comparison of the proposed approach and the Grodecki's original approach using IKONOS images

demonstrates that the elevation constraints improve the relative accuracy of RFM block adjustment. When using the proposed approach, the following suggestions are offered.

1) If no accurate DEM is available when block adjusting single-line-array images, GCPs should be distributed in each orbit.
2) When the adjusted images have relatively large side sways, using denser ETPs can reduce the influence of DEM error and may improve the accuracy of block adjustment.
3) If the purpose of block adjustment is to produce orthomosaics, the DEM used for orthorectification should also be used in the block adjustment to interpolate the elevations of tie points.

ACKNOWLEDGMENT

The authors would like to thank Suzhou Image Sky Company for providing the ZY-3 test data and topographic data, as well as ESRI for testing the approach with the IKONOS-2 image.

REFERENCES

[1] T. Toutin, "Block bundle adjustment of IKONOS in-track images," *ISPRS J. Photogramm. Remote Sens.*, vol. 24, no. 4, pp. 851–857, 2003.
[2] A. Bouillon *et al.*, "SPOT 5 HRS geometric performances: Using block adjustment as a key issue to improve quality of DEM generation," *ISPRS J. Photogramm. Remote Sens.*, vol. 60, no. 3, pp. 134–146, May 2006.
[3] Y. Zhang, M. Zheng, J. Xiong, Y. Lu, and X. Xiong, "On-orbit geometric calibration of ZY-3 three-line array imagery with multistrip data sets," *IEEE Trans. Geosci. Remote Sens.*, vol. 52, no. 1, pp. 224–234, Jan. 2014.
[4] Y. Zhang *et al.*, "Fully automatic generation of geoinformation products with Chinese ZY-3 satellite imagery," *Photogramm. Rec.*, vol. 29, no. 148, pp. 383–401, Dec. 2014.
[5] J. Grodecki, "IKONOS stereo feature extraction—RPC approach," in *Proc. ASPRS Annu. Conf.*, 2001, pp. 23–27.
[6] J. Grodechi and G. Dial, "Block adjustment of high-resolution satellite images described by rational polynomials," *Photogramm. Eng. Remote Sens.*, vol. 69, no. 1, pp. 59–68, 2003.
[7] C. Fraser, G. Dial, and J. Grodecki, "Sensor orientation via RPCs," *ISPRS J. Photogramm. Remote Sens.*, vol. 60, no. 3, pp. 182–194, May 2006.
[8] Z. Xiong and Y. Zhang, "A generic method for RPC refinement using ground control information," *Photogramm. Eng. Remote Sens.*, vol. 75, no. 9, pp. 1083–1092, 2009.
[9] T.-A. Teo, L.-C. Chen, C.-L. Liu, Y.-C. Tung, and W.-Y. Wu, "DEM-aided block adjustment for satellite images with weak convergence geometry," *IEEE Trans. Geosci. Remote Sens.*, vol. 48, no. 4, pp. 1907–1918, Apr. 2010.
[10] T. Toutin, "Block bundle adjustment of Landsat 7 ETM+ images over mountainous areas," *Photogramm. Eng. Remote Sens.*, vol. 69, no. 12, pp. 1341–1349, 2003.
[11] T. Toutin, "Spatiotriangulation with multisensor VIR/SAR images," *IEEE Trans. Geosci. Remote Sens.*, vol. 42, no. 10, pp. 2096–2103, Oct. 2004.
[12] T. Toutin, "Spatiotriangulation with multisensor HR stereo-images," *IEEE Trans. Geosci. Remote Sens.*, vol. 44, no. 2, pp. 456–462, Feb. 2006.
[13] C. S. Fraser and M. Ravanbakhsh, "Georeferencing accuracy of GeoEye-1 imagery," *Photogramm. Eng. Remote Sens.*, vol. 75, no. 6, pp. 634–638, 2009.
[14] T. Wang *et al.*, "Planar block adjustment and orthorectification of ZY-3 satellite images," *Photogramm. Eng. Remote Sens.*, vol. 80, no. 6, pp. 559–570, Jun. 2014.
[15] D. Li, "China's first civilian three-line-array stereo mapping satellite: ZY-3," *Acta Geodaetica et Cartographica Sinica*, vol. 41, no. 3, pp. 317–322, 2012.
[16] J. Grodecki and G. Dial, "IKONOS geometric accuracy," in *Proc. Joint Int. Workshop High Resolution Mapping Space*, 2001, pp. 19–21.
[17] Y. Zhang, Y. Lu, L. Wang, and X. Huang, "A new approach on optimization of the rational function model of high-resolution satellite imagery," *IEEE Trans. Geosci. Remote Sens.*, vol. 50, no. 7, pp. 2758–2764, Jul. 2012.
[18] G. Sun, K. Ranson, V. Kharuk, and K. Kovacs, "Validation of surface height from Shuttle Radar Topography Mission using shuttle laser altimeter," *Remote Sens. Environ.*, vol. 88, no. 4, pp. 401–411, Dec. 2003.
[19] C. G. Brown, K. Sarabandi, and L. E. Pierce, "Validation of the Shuttle Radar Topography Mission height data," *IEEE Trans. Geosci. Remote Sens.*, vol. 43, no. 8, pp. 1707–1715, Aug. 2005.
[20] S. J. Wright and J. Nocedal, *Numerical Optimization*. New York, NY, USA: Springer-Verlag, 1999, pp. 245–269.
[21] S. Agarwal, N. Snavely, S. M. Seitz, and R. Szeliski, "Bundle adjustment in the large," in *Computer Vision-ECCV*. Berlin, Germany: Springer-Verlag, 2010, pp. 29–42.
[22] M. Byröd and K. Åström, "Conjugate gradient bundle adjustment," in *Computer Vision-ECCV*. Berlin, Germany: Springer-Verlag, 2010, pp. 114–127.
[23] Y. Sheng, "Theoretical analysis of the iterative photogrammetric method to determining ground coordinates from photo coordinates and a DEM," *Photogramm. Eng. Remote Sens.*, vol. 71, no. 7, pp. 863–871, Jul. 2005.
[24] Y. Sheng, "Modeling algorithm-induced errors in iterative monoplotting process," *Photogramm. Eng. Remote Sens.*, vol. 74, no. 12, pp. 1529–1537, 2008.

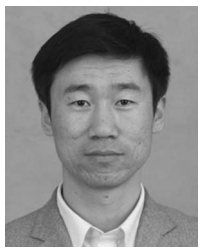

Yongjun Zhang was born in 1975. He received the B.S., M.S., and Ph.D. degrees from Wuhan University, Wuhan, China, in 1997, 2000, and 2002, respectively.

He is currently a Professor of photogrammetry and remote sensing with the School of Remote Sensing and Information Engineering, Wuhan University. His research interests include space, aerial, and low-altitude photogrammetry, image matching, combined bundle adjustment with multisource data sets, 3-D city reconstruction, and industrial inspection.

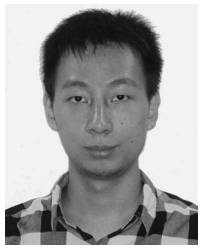

Yi Wan was born in 1991. He received the B.S. degree in 2013 from Wuhan University, Wuhan, China, where he is currently working toward the Ph.D. degree.

His research interests include photogrammetry and geometric analysis and processing of remote sensing data.

Xinhui Huang was born in 1990. She received the B.S. and M.S. degrees from Wuhan University, Wuhan, China, in 2012 and 2015, respectively.

Since 2015, she has been with StarGIS co., Ltd, Tianjin, China. Her research interests include image quality assessment and processing of remote sensing data.

Xiao Ling was born in 1989. He received the B.S. and M.S. degrees in 2012 and 2014, respectively, from Wuhan University, Wuhan, China, where he is currently working toward the Ph.D. degree.

His research interests include photogrammetry and image matching.